Journal of Process Control 19 (2009) 415–432

Contents lists available at ScienceDirect

Journal of Process Control

journal homepage: www.elsevier.com/locate/jprocont

Control of the mass and energy dynamics of polybenzimidazole-membrane fuel cells

Federico Zenith *, Sigurd Skogestad

Department of Chemical Engineering, Norwegian University of Science and Technology, Sem Sælands veg 4, 7491 Trondheim, Norway

ARTICLE INFO

Article history:
Received 29 November 2007
Received in revised form 17 June 2008
Accepted 21 June 2008

Keywords:
Fuel cell
Dynamics
Control

ABSTRACT

The dynamic modes related to mass and energy of a high-temperature proton-exchange-membrane fuel cell are investigated. For a particular configuration, three lumped-parameters dynamic equations are considered to represent hydrogen pressure in the anode, oxygen fraction in the cathode, and stack temperature. For each of these, a simple controller algorithm is developed. These algorithms are tested against a standard driving cycle for vehicles, and are found to be able to maintain the necessary conditions for the fuel cell stack to operate. It is possible to control temperature by using only air cooling, without significant additional requirements on air flow manipulation.

1. Introduction

A fuel cell is a device capable of converting chemical energy stored in fuels, such as hydrogen, methanol or formic acid, directly into direct-current electricity without the combustion step required by thermal cycles. Fuel cells have been the subject of extensive research in later years, because of the several potential advantages over today's combustion engines: fuel cells are theoretically more efficient, can be easily scaled up by stacking several cells in various configurations, do not have major moving parts and run silently. When run on hydrogen, they produce only water as a by-product.

The literature produced in the recent decades about various aspects of fuel cells is too extensive to be comprehensively reviewed in this paper; the interested reader is referred to available textbooks [1].

The literature on dynamics of fuel cells can be confusing. Sometimes the dynamics are claimed to be sluggish and unresponsive, requiring several minutes to settle [2], whereas other authors state that the dynamics is fast and that control is unproblematic [3].

The reason behind these apparently contradicting results is the interdisciplinarity of fuel cells: fuel cell systems require modelling in the domains of chemical engineering (for mass and energy balances), electrochemistry (for reaction kinetics and diffusion in the gas-diffusion layers), and electrical engineering (for power conversion of the direct current obtained from the cell stack), as shown in Fig. 1.

It is important to remark that, for the end user, the actual power delivery is the only relevant metrics of system performance: any slow dynamics inside the system should be hidden from the user through automatic control, and, as long as these do not interfere with the performance of the last leg of the graph in Fig. 1, they will be of no consequence to the user. This is not to say that the slow dynamics and control of these are unimportant, as they are actually the main topic of this paper.

Many types of fuel cells have been proposed, of which the solid-oxide fuel cell and the proton-exchange-membrane (PEM) fuel cell are the most commonly reported in the recent literature. This paper will focus on a particular subset of PEM fuel cells, namely those with a membrane of polybenzimidazole instead of the more common Nafion. These cells operate at temperatures higher than 100 °C and up to 200 °C, and do not rely on water for proton conductivity: they are therefore free of the water-management problems of Nafion membranes caused by the presence of liquid water, whose quantity has to be kept in a narrow window of acceptable values. A comprehensive review of high-temperature PEM fuel cells has been published by Zhang et al. [4].

In a previous article [5], we investigated the electrochemical transients in a polybenzimidazole-membrane fuel cell, and the main result was that these dynamics pose no fundamental limits to controllability. The power output was controlled by manipulating a DC/DC buck-boost converter [6], by means of logical switching rules. This paper is therefore concerned with the first block of the graph in Fig. 1, namely the relatively slow transients associated with the mass and energy balances.

* Corresponding author. Present address: Max Planck Institute for Dynamics of Complex Technical Systems, Sandtorstraße 1, 39106 Magdeburg, Germany. Tel.: +49 391 6110 166.
E-mail addresses: zenith@mpi-magdeburg.mpg.de (F. Zenith), skoge@chemeng.ntnu.no (S. Skogestad).

0959-1524/$ - see front matter © 2008 Elsevier Ltd. All rights reserved.
doi:10.1016/j.jprocont.2008.06.019

Nomenclature

A	area (m^2)
c_p	molar heat capacity (J/mol K)
$\hat{c}_p$	areal heat capacity (J/m^2 K)
C_{rf}	rolling friction coefficient (–)
C_d	drag coefficient (–)
F	Faraday constant (C/mol)
g	gravitational acceleration (m/s^2)
h	specific enthalpy (J/mol)
H	enthalpy (J)
$\dot{H}$	enthalpy flow (W)
i	current density (A/m^2)
m	mass (kg)
n	number of moles (mol)
$\dot{n}$	molar flow (mol/s)
p	pressure (Pa)
P	power (W)
R	ideal gas constant (J/mol K)
s	Laplace variable (rad/s)
t	time (s)
T	temperature (K)
v	velocity (m/s)
V	voltage (V)
W	volume (m^3)
x	molar fraction (–)
X	conversion (–)

Greek symbols

θ	delay (s)
ν	stoichiometric coefficient (–)
ρ	density (kg/m^3)
τ	time constant (s)

Superscripts

in	entering
out	exiting
c	combustion

Subscripts

r	reaction
m	measurement
tot	total

2. Literature review on control of fuel cells

Many papers about fuel cells have been published about the development of appropriate materials, steady-state system analysis, but these rarely touch the issues of dynamics or control of the fuel cell system.

Some early interest in control of fuel cells arose in the late sixties, when the main issue being investigated was controlling the concentration of hydrazine or methanol in alkaline fuel cells [7,8], then considered a viable portable power source for battlefield military applications. The issue was complicated by the difficulty of measuring the actual reactant concentration in the electrolyte, which was the main problem being debated at the time. Ang et al. [8] suggested, for example, to use a dedicated measuring cell. However, these papers did generally not contain much control theory (if any at all), and their focus on hydrazine- and methanol-fuelled alkaline fuel cells make them of little relevance for today's mostly hydrogen-fuelled PEM fuel cells.

One of the first dynamic models for fuel cell systems was published by He [9]. He considered a molten-carbonate fuel cell stack fed with reformate hydrogen, and focused mostly on mass flows and energy balance of the pre-processing plant and of the cell stack. The electrochemical model was comparatively simple, with no dynamics and being, essentially, a Thevenin equivalent circuit with a voltage generator and a resistance.

A dynamic model for PEM fuel cells by Amphlett et al. [10] appeared in 1996, and was subsequently cited in a large number of papers. It was a thermal model with a basic, empirical modelling of the overvoltage effects. Current was considered a system input, and the catalytic overvoltage was assumed to vary instantly as a function of temperature, oxygen concentration and current. The model predicts well the behaviour of the stack in a time scale of minutes, but, since it does not consider the transient in overvoltage, it might be less accurate in the scale of seconds and lower.

Two similar US patents have been granted to Lorenz et al. [11] and Mufford and Strasky [12], both concerning methods to control the power output of a fuel cell. Both these methods use air inflow as the input variable. Whereas this variable can indeed be set by manipulating the air-compressor speed, there are various reasons why this choice of input variable is not the best option. First of all, only the fuel cell itself is considered: no information from the utility that will draw power from the cell is being used. Also, while it could seem intuitive that a fuel cell will produce more power the more oxidant it is fed, this neglects a series of phenomena such as the mass-transport limit, the strong nonlinear effects of oxygen partial pressure in cathode kinetics, diffusion of oxygen through the cathode and accumulation of oxygen in the cathode manifold; in short, a fuel cell cannot always output as much power as the reactant it is fed.

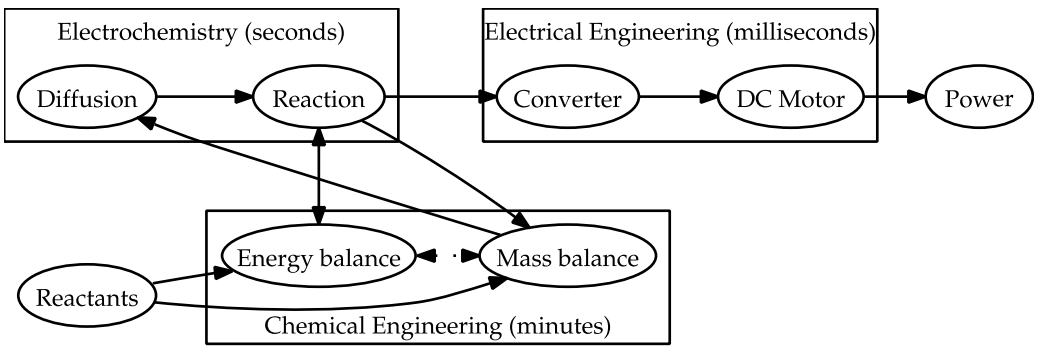

Fig. 1. The main dynamic modes of a fuel-cell system.

Rune Johansen, a student at the Department of Materials Technology at NTNU, investigated in his master's thesis [13] the possibility of using reactant feed rate as a means to control power output from a fuel cell. His results indicate that there is a significant delay during which reactants in the manifolds must be depleted before the effect of an interrupted reactant inflow on the power output can be apparent; the actual extent of this delay will depend, among other things, on the sizing of the manifolds and on the rate of consumption of reactants; on the other hand, there is no such delay when the reactant flow is restored. Johansen's findings indicate that the feed rate of reactants is a poor control input for power-output control. Because of the delays, nonlinearities and asymmetries associated with the input's effect on the system, the system's performance in reference tracking and disturbance rejection will be severely limited. Furthermore, such a starvation strategy would be energetically inefficient.

The approach of controlling power output by manipulating inlet flows has also been experimentally investigated by Woo and Benziger [2]. In their layout, a PEM fuel cell was fed oxygen or air on the cathode side, and pure hydrogen for the anode; all outlet gas streams had to bubble through a water column. When reducing the hydrogen flow below the requirements, the reduction of hydrogen pressure caused water to enter the cell and cover parts of the anode, effectively producing a variable-area cell. The control action resulted in transients in the order of magnitude of 10 s.

The PhD thesis by Pukrushpan [14] and an article by the same author and others [15] are among the first important contributions to control of PEM fuel cells. Most of the focus is on air-inflow control, with a significant section about control and modelling of natural-gas fuel processors.

Serra et al. [16] used linear-control analysis to synthesise controllers for a fuel cell at different linearisation points. They used Pukrushpan's model [14], and their objective was to control the voltage of a large stack by manipulating valve positions, reactant input and humidification. They concluded that few of these controllers had a wide operating range.

Caux et al. [17] considered a system comprising a fuel cell, a compressor, valves, and two DC/DC converters (a booster and a buck-boost converter). The analysis of the complete system is a step forward from the studies in which the fuel cell had been seen as a separate entity from the rest of the process, but the fuel cell model itself is the same as from Amphlett et al. [10], and is therefore not considering transients in overvoltage; voltage variations will therefore be caused, directly, only by variations in temperature, current or oxygen concentration. A similar layout was investigated by Thounthong et al. [18,19], with more focus on power electronics control and less on cell modelling, and some experimental results.

Williams et al. [3] tested the dynamic performance of a fuel cell stack connected to a DC/DC converter controlled with pulse-width modulation. They tested the system in a range of frequencies between 1 and 400 Hz, and claimed that the bandwidth of the fuel cell system was quite high, about 50 Hz, when controlling it with a PI controller.

Choe et al. [20] should probably be credited with the first paper that explicitly considers more than one aspect of the dynamics of a fuel cell, namely both converter dynamics and reactant management, applied to a low-temperature PEM fuel cell.

3. Process description

This paper will analyse some of the dynamic modes of fuel cells, and will propose simple algorithms to control these appropriately. This paper is based on the yet unpublished parts of the first author's PhD. thesis [21].

There are many possible designs for fuel cells, but for our control study we will consider a fairly simple PBI-membrane fuel cell system running on pure hydrogen and air. Hydrogen enters a "dead-end" manifold on the anode side. Air, on the other hand, needs an outlet to let produced water vapour and accumulated nitrogen flow out, and therefore passes through an open-end manifold on the cathode side. The entering flows of hydrogen and air are assumed to be manipulable. The process is sketched in Fig. 2.

To keep the complexity to a minimum, we will consider a lumped-parameter model for the whole stack: the variables we shall consider are hydrogen pressure at the anode, oxygen concentration at the cathode, electrochemical overvoltage and temperature, which we all assume uniform throughout all cells in the stack.

These assumptions, however, have different degrees of credibility. Hydrogen pressure is likely to be fairly equalised in the system, as a difference in pressure would rapidly be compensated by flow to the regions of lower pressure. An uniform pressure at the anode is probably an accurate approximation of reality. It must be noted, though, that nitrogen and water crossover and the presence of impurities in the feed hydrogen will cause a build-up of inert gases in the anode, that will have to be periodically purged; in this paper, we assume that the effects of purging are beyond the bandwidth of interest.

The assumption of uniform oxygen concentration at the cathode, on the other hand, requires a parallel flow layout, where entering air is fed in parallel to all cells and goes to the outlet after a single pass. Since the main disturbance to oxygen concentration, the reaction rate, is proportional to the current passing through the cell stack, it will have the same value in all the cells, which are usually electrically connected in series to increase the stack voltage.

The series configuration is often used to mechanically purge product water from Nafion-based PEM fuel cells, but is practical only for small numbers of cells due to the rapidly increasing pressure drop; besides, as we are considering a PBI-based cell stack, we are not concerned with water removal. We will therefore consider an air network in a parallel Z configuration, as described by Karimi et al. [22], which consists of equally long paths from inlet to outlet through each cell.

Uniform cathodic concentrations also implies that concentration gradients through each cathodic side are negligible; in reality, the progressive consumption of oxygen along the flow channels from the inlet to the outlet of each cell will result in an average concentration higher than the one we calculate: in our uniform-concentration approximation we are assuming that oxygen concentration is everywhere the lowest one, i.e. the outlet concentration. Since we are usually concerned about maintaining a minimum oxygen concentration in the cells, this approximation is considered to be conservative.

The least likely assumption is probably the uniform stack temperature. According to Shan and Choe [23,24], the temperature profile across a single Nafion-based cell, and even across an entire stack, is fairly uniform. However, it remains to be investigated

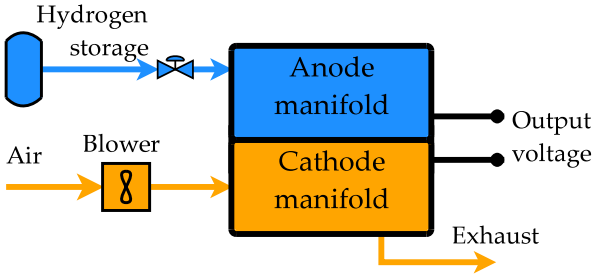

Fig. 2. The process being modelled: a fuel cell stack running on pure hydrogen and air at atmospheric pressure, with no anode outlet, and with polybenzimidazole proton-conducting membranes.

whether these results apply also to PBI cells, which are run at higher temperatures. Furthermore, the temperature profile could deviate even more from uniformity during transients.

The electrochemical model assumed in this paper is the one previously presented by the same authors and others [5]; the reader is referred to our previous publication for its details and assumptions. One of the most important assumptions is that the PBI membrane's conductivity does not depend on humidity nor temperature; we will use a value measured at 150 °C, but further investigations should include a model of the effects of temperature on conductivity: in fact, since the membrane's conductivity can be very dependent on temperature, the cell's polarisation and specific-power curves presented in this paper may significantly change with temperature.

4. Dynamic model

4.1. Hydrogen inventory (dead-end flows)

Some mass balances do not need an outlet, since all of the entering flow is consumed by chemical reactions on that side of the fuel cell.

For the case of an anode fed on pure hydrogen, the equation of mass conservation is simply

$$\frac{dn_{H_2}}{dt} = \dot{n}_{H_2} - \frac{i_r A}{2F} \tag{1}$$

where $\dot{n}_{H_2}$ is the feed stream and we have assumed there is no exit stream. Assuming that the ideal gas law is valid, $n_{H_2} = \frac{p_{H_2} W}{RT}$, which upon differentiation gives

$$\frac{dn_{H_2}}{dt} = \frac{W}{RT}\left(\frac{dp_{H_2}}{dt} - \frac{p_{H_2}}{T}\frac{dT}{dt}\right) \tag{2}$$

Substituting this into the mass balances gives

$$\frac{dp_{H_2}}{dt} = \frac{RT}{W}\left(\dot{n}_{H_2} - \frac{i_r A}{2F}\right) + \frac{p_{H_2}}{T}\frac{dT}{dt} \tag{3}$$

For control purposes, the last term may be neglected if temperature transients are sufficiently slow, since transients in pressure are typically much faster than the ones in temperature.

In a real system there are always some impurities in the hydrogen feed and some periodic purging will be necessary even for dead-end flows. This has not been modelled here. If the fraction of impurities in the entering flow is significant, as could be the case for hydrogen produced by steam reforming, an open-end flow layout is more appropriate.

4.2. Oxygen and water inventory (open-end flows)

If the feed contains some inert components, or if there are reaction products, an outlet is required to remove these species. In PEM fuel cells, this is the case for the cathode, as water is generated by the reaction. In addition, for the important case of air-fed cells, inerts in the form of nitrogen are present.

4.2.1. Diffusion limits

The main problem posed by inert gases is the presence of diffusion limits. Simplifying the Stefan–Maxwell equations, an approximate limit to the reaction current has been obtained in our previous work [5], considering only the cathode. At this limiting current, the steady-state partial pressure of oxygen at the reaction surface reaches zero; this limit is known as the mass-transport barrier in the literature.

For small oxygen concentrations, this limiting current is proportional to the partial pressure of oxygen in the bulk. Even if the cell is fed pure oxygen, however, the mass-transport barrier will not disappear, as water still has to exit the diffusion layer. To increase the current limit and allow more power output from the cell, therefore, it is necessary to increase the fraction of oxygen in the cathode gases. The simplest approach is to increase the inlet flow rate to purge inerts and bring oxygen closer to its inlet concentration.

4.2.2. Effects of bulk oxygen concentration

The partial pressure of oxygen in the cathode's bulk influences the shape of the cell's polarisation curve, and a series of simulations has been performed with data and parameters from our previous publication [5] in Fig. 3.

For the reaction $O_2 + 2H_2 \rightarrow 2H_2O$, the steady-state mass balance at the cathode side gives

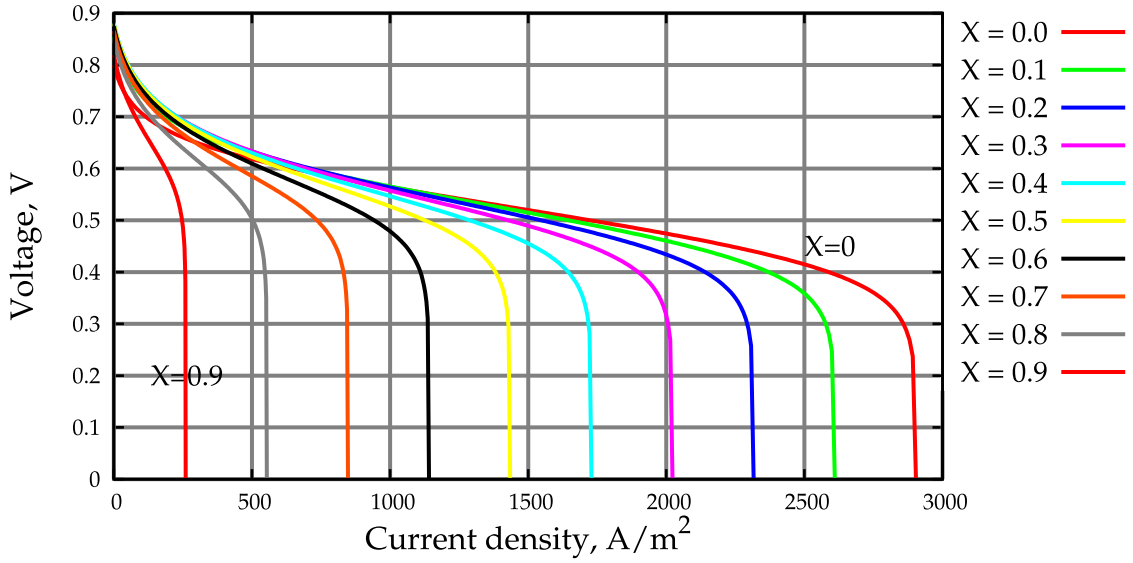

Fig. 3. Polarisation curves of a fuel cell as a function of oxygen conversion, data from our previous publication [5].

$$\begin{cases} n_{O_2} = n_{O_2}^{in}(1-X) \\ n_{N_2} = n_{N_2}^{in} \\ n_{H_2O} = n_{H_2O}^{in} + 2n_{O_2}^{in}X \\ n_{tot} = n_{tot}^{in} + n_{O_2}^{in}X \end{cases} \quad (4)$$

Here X is oxygen conversion and n_i^{in} is the number of moles of component i in the inlet stream. The corresponding outlet molar fractions n_i/n_{tot} become

$$\begin{cases} x_{O_2} = \frac{x_{O_2}^{in}(1-X)}{1+x_{O_2}^{in}X} \\ x_{N_2} = \frac{x_{N_2}^{in}}{1+x_{O_2}^{in}X} \\ x_{H_2O} = \frac{x_{H_2O}^{in}+2x_{O_2}^{in}X}{1+x_{O_2}^{in}X} \end{cases} \quad (5)$$

We assume that the feed has a total pressure of 101 325 Pa (a standard atmosphere). The partial pressure of water in the feed is assumed to be 1700 Pa, which is the vapour pressure of water at approximately 15 °C, or a relative humidity of 53% at 25 °C. Dry air is assumed to be made up of 20% oxygen and 80% nitrogen.

Note that the mass-transport current limit recedes almost linearly with conversion. The corresponding power output (current times voltage) is shown in Fig. 4.

The maximum power outputs for the curves in Fig. 4 are shown in Fig. 5 as a function of conversion, along with the corresponding oxygen and water molar fractions. It is noticeable that the maximum available power varies almost linearly with these variables.

These results are valid for a fuel cell whose cathodic bulk partial pressures are as given by equation set (5). This is the case for a fuel cell whose open-end cathode manifold operates as a steady-state CSTR reactor (with perfect mixing), and with no perturbations in the entering composition.

Fig. 5 can therefore be used to derive a simple rule-of-thumb for fuel cells of the type investigated in this article: a fuel cell's maximum power output is approximately proportional to the oxygen partial pressure. This implies that the air flow in the cathode should be large in order to produce more power.

4.2.3. Dynamic mass-balance equations for open-end flows

For a generic species i, the dynamic mass balance on molar basis on an open-end flow is

$$\frac{dn_i}{dt} = \dot{n}^{in}x_i^{in} - \dot{n}^{out}x_i + \overbrace{\nu_i\frac{i_r A}{F}}^{\text{Reaction}} \quad (6)$$

The stoichiometric factor ν_i indicates how many moles of the species are produced or consumed for every mole of electrons transferred. Since the anodic and cathodic reactions are, respectively,

$$\begin{aligned} &\frac{1}{2}H_2 \rightarrow H^+ + e^- \\ &\frac{1}{4}O_2 + H^+ + e^- \rightarrow \frac{1}{2}H_2O \end{aligned} \quad (7)$$

we have $\nu_{O_2} = -\frac{1}{4}$, $\nu_{H_2} = -\frac{1}{2}$, $\nu_{H_2O} = \frac{1}{2}$ and $\nu_{N_2} = 0$.

Summing up for all components and assuming constant pressure, the total molar balance becomes

$$\dot{n}^{out} = \dot{n}^{in} + \sum_i \nu_i\frac{i_r A}{F} - \frac{dn}{dt} \quad (8)$$

where index i stands for a generic species in the flow.

Combining this with the component balance (6), using $\frac{dn_i}{dt} = x_i\frac{dn}{dt} + n\frac{dx_i}{dt}$, the molar balance becomes for each species i:

$$n\frac{dx_i}{dt} = \dot{n}^{in}(x_i^{in} - x_i) + \frac{i_r A}{F}\left(\nu_i - x_i\sum_j \nu_j\right) \quad (9)$$

where index j stands for a generic species in the flow.

Fortunately, the expansion term $\frac{dn}{dt}$ cancels out. This is a set of differential equations in the molar fractions x_i. In a control setting, we can view $\dot{n}^{in}$ as the manipulated variable, since it can be set with an air blower or a compressor, and i_r as a disturbance, since it is a consequence of the external load connected to the fuel cell.

4.3. Energy balance

The temperature dynamics are important for PEM fuel cells. Nafion-based PEM cells operate in a narrow temperature range, usually around 80 °C (more if pressurised), whereas PBI membranes can operate in a much wider range, from 125 to 200 °C. High temperatures may be exploited to reduce the catalytic overvoltage due to reaction kinetics, or to increase tolerance to catalyst poisons such as CO.

Assuming constant pressures at both the cathode and the anode, we have $\frac{dU}{dt} = \frac{dH}{dt}$, and an energy balance for the stack yields

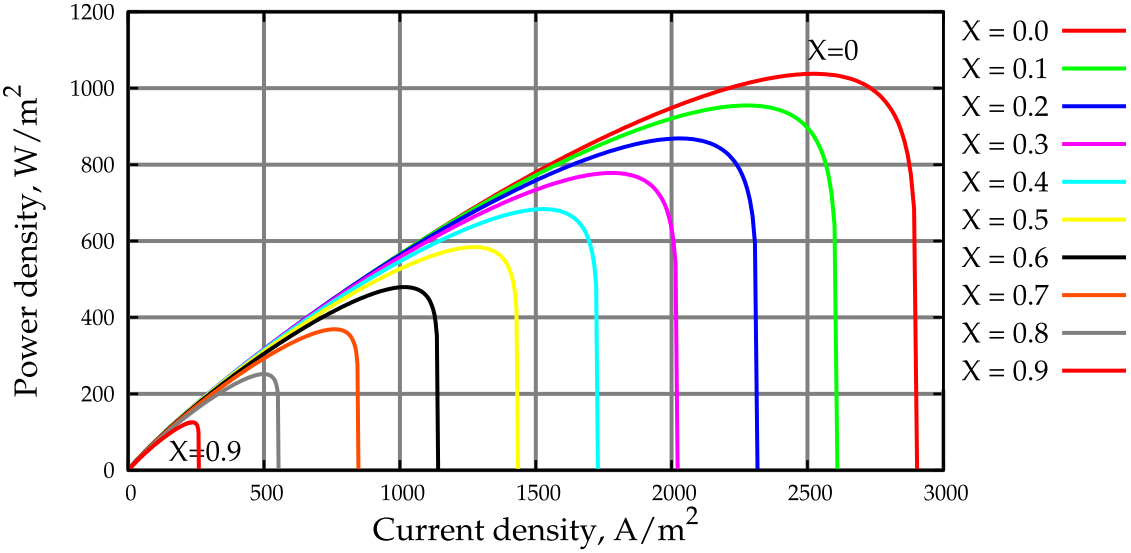

Fig. 4. Effect of conversion on the cell's power output delivered to the load. This figure represents the same data as Fig. 3, with power density defined by $\frac{P}{A} = iV$.

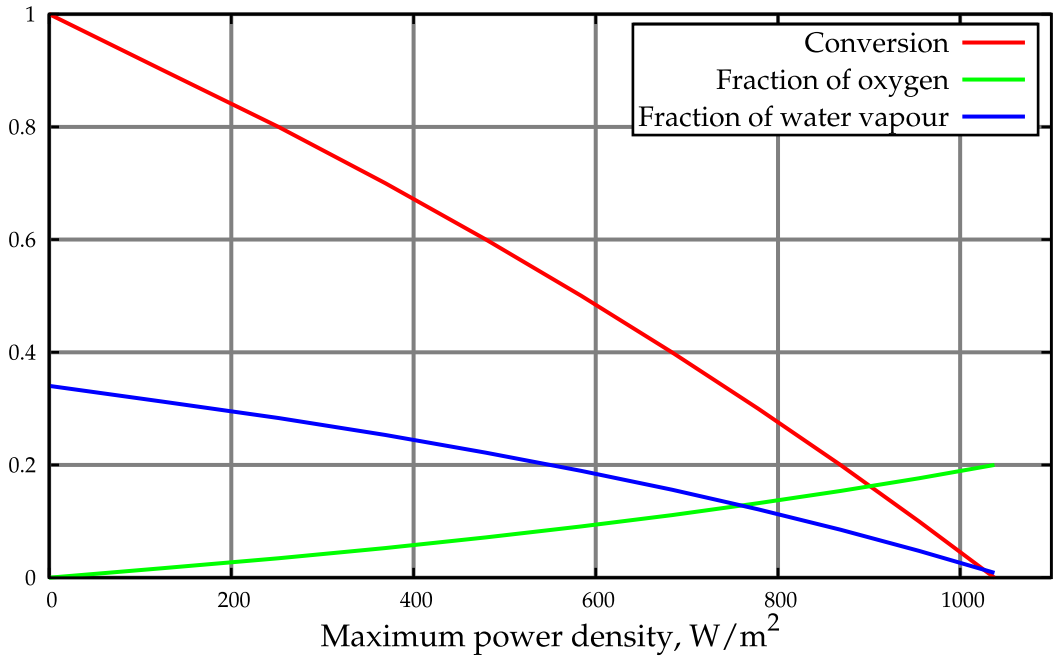

Fig. 5. Relationship between the maximum power output and conversion.

$$\frac{dH}{dt} = \dot{H}^{in} - \dot{H}^{out} - \overbrace{i_r VA}^{\text{Electric power}} - \dot{H}^{loss} \tag{10}$$

Neglecting the mass of the gas compared to the cell's solid components, we have that the heat capacity per cell area is about 7 kJ/K m^2 [23].

$$\frac{dH}{dt} = A\hat{c}_p \frac{dT}{dt} \tag{11}$$

The entering enthalpy flow is associated with the entering air and hydrogen:

$$\dot{H}^{in} = \dot{n}_{air} h_{air}(T^{in}) + \left(\dot{n}_{H_2} + \dot{n}^{c}_{H_2}\right) h_{H_2}\left(T^{in}_{H_2}\right) \tag{12}$$

Here $\dot{n}^{c}_{H_2}$ denotes the extra hydrogen burnt in the cathode inlet during start-up. The entering hydrogen temperature T^{in}_{H2} can be significantly different from the ambient temperature T^{in}, as hydrogen from storage could undergo an expansion, be evaporated from liquid state, or heated in order to dissociate it from hydrides. Modelling the dynamics of hydrogen inlet temperature is beyond the scope of this article, and we will for simplicity assume that hydrogen has been brought to ambient temperature ($T^{in}_{H2} = T^{in}$).

We assume that the only output flow is at the cathode. The cathode gas composition will change as oxygen is consumed, and the total outlet molar flow will be larger or equal than the entering one.

$$\dot{H}^{out} = \sum_i \dot{n}^{out}_i h_i(T) \tag{13}$$

Here, for a generic species i in the cathodic flow, $\dot{n}^{out}_i = x_i \dot{n}^{out}$ where x_i is given by integrating Eq. (9), and $\dot{n}^{out}$ is given by (8). The functions $h_i(T)$ depend on the temperature T of the cell's cathode.

The heat loss to the environment, $\dot{H}^{loss}$, is generally favourable as it removes heat from the stack. However, its actual expression will depend on the stack materials and construction, and for sake of simplicity we will assume $\dot{H}^{loss} = 0$. It should be noted, though, that even low heat losses could lead to water condensation during periods of low power output; the study of such conditions is however beyond the scope of this paper.

5. Control implementation

5.1. Power requirements

In order to evaluate the performance of alternative control algorithms, it is useful to have a standard usage pattern against which to test them. Since fuel cells are often associated with automotive applications, we use the New European Driving Cycle (NEDC), a standard velocity-to-time map used in the European Union to test car engines for pollutant emissions [25,26]. The NEDC is representative of both urban and extra-urban driving in Europe, but many other countries and authorities have defined their own set of driving cycles, such as the United States' FTP-75 and Japan's JP 10–15.

Having obtained the $v(t)$ relationship from the definition of NEDC, it is possible to obtain the corresponding motor power output by making some assumptions on the characteristics of the vehicle. It is then possible, through the power characteristic of the fuel cell, to find a corresponding map for $i(t)$ and $V(t)$, thereby finding the main disturbance terms in all flow and heat differential equations (1), (9), and (10).

The velocity specified by the NEDC standard is plotted in Fig. 6, with the corresponding power required by the vehicle to maintain the specified velocity. The power the motor has to output to make the vehicle maintain the cycle's specified velocity can be calculated as follows [13]:

$$P = \overbrace{mgC_{rf}|v|}^{\text{Rolling resistance}} + \overbrace{\frac{1}{2}\rho|v|^3 C_d A}^{\text{Air resistance}} + \overbrace{mv\frac{dv}{dt}}^{\text{Acceleration}} \tag{14}$$

This equation represents the power requirement of the vehicle that the fuel cell stack will have to match. The parameters used in this equation are presented in Table 1.

With the expression for the required power output, we can now estimate the current i by inverting the $P(i)$ relationship of the fuel cell stack. However, the fuel cell's polarisation curve (and with it its power output) depends strongly on oxygen conversion X in the cathode, as shown in Fig. 3. To invert the relationship $P(i,X)$ it is therefore first necessary to assume a value for conversion. Fig. 5 indicates that conversion must be low for the highest power

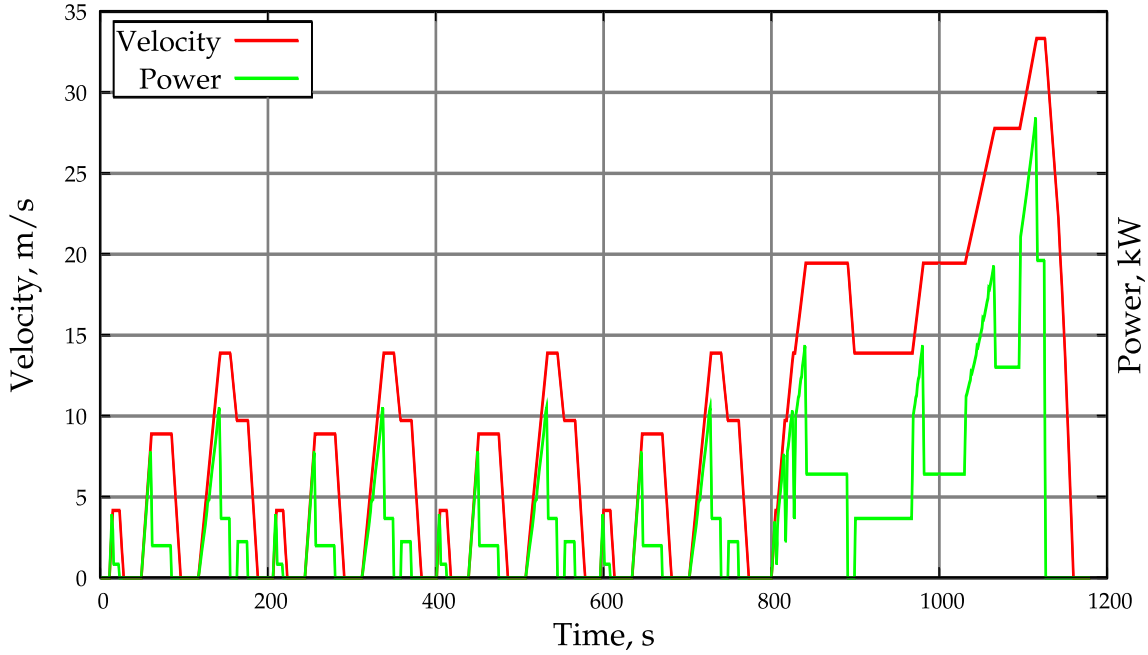

Fig. 6. The New European Driving Cycle. Negative values of power have been discarded, as we are not considering the possibility of inverting the fuel cells and using them as electrolysers.

Table 1
The parameters used to find the power requirements of a vehicle following the NEDC cycle

Symbol	Unit	Value
m	Mass	1000 kg
g	Gravitational acceleration	9.81 m/s^2
ρ	Air density	1.177 kg/m^3
C_{rf}	Rolling friction coefficient	0.02
C_d	Drag coefficient	0.4
A_v	Vehicle front area	1.5 m^2

outputs to be attainable. Furthermore, as shown in Fig. 4, the power output curves do not depend significantly on X until the mass-transport barrier is actually reached for each curve: each curve then separates from a common envelope quite suddenly. We will therefore consider this envelope ($X = 0$) a representative estimate to invert $P(i,X)$, because we assume that control will be able to keep the stack away from the mass-transport limit.

We can now find the rate of oxygen consumption, $\frac{i_r(t)A}{4F}$, and heat generation, $\left[\frac{\Delta h_f}{2F} - V(t)\right] i_r(t)$. In all of the following simulations we assume that the fuel cell stack has a total area of 30 m^2, resulting in a theoretical maximum power output of 31.13 kW, or 9.5% more than the maximum required power by NEDC, which is 28.42 kW. The oxygen consumption and heat generation are plotted in Fig. 7, where we can see that they quite closely match the shape of power requirement in Fig. 6.

5.2. Power-output control

The easiest way to control the power output is to connect the fuel cell stack with an adjustable external circuit, be it a rheostat, a MOSFET, or a DC/DC converter. Details about converter control and overvoltage dynamics in a control-oriented setting may be found in our previous publication in this journal [6], and will not be discussed further here.

As noted in our earlier publication, power output may be perfectly controlled, with closed-loop response times in the millisecond range. However, a sustainable power output from a fuel cell requires that resources, in terms of hydrogen and oxygen, are available, and also that temperature is controlled.

5.3. Hydrogen-pressure control (anode)

Sustaining the power output and reaction rate requires maintaining a steady supply of reactants. Since the dead-end anode manifold has only one way in for hydrogen (the inlet) and one way out (reaction), we will try to control the quantity of hydrogen in the anode side by manipulating the inflow, in spite of variations in the reaction rate required by the user. The easiest way to control the amount of hydrogen present in our system is to maintain a constant pressure.

We will assume that the hydrogen inflow can be directly manipulated. It would also be possible to manipulate the opening of a valve connected to a higher-pressure reservoir, but the mathematical modelling would be more complex while providing little additional insight. Furthermore, the various possible types of hydrogen storage may have different and more complex modelling than a throttling valve's: this may include evaporation and heat transfer in liquid-hydrogen storage, desorption dynamics in metal-hydride storage, or other aspects that we will not explore here.

The dynamic model is given in Eq. (3), where we neglected the term accounting for temperature variation.

$$\frac{dp_{H_2}}{dt} = \frac{RT}{W}\dot{n}_{H_2} - \frac{RT}{W}\frac{i_r A}{2F} \tag{15}$$

Since the system's state p_{H_2} does not appear in the right-hand side, this is an integrating process. As integrating processes are not stable, feedback is mandatory: if there were no pressure measurement, and we only relied on a current measurement to set the flow to compensate consumption, any error would accumulate over time, and we would eventually either run out of hydrogen or rupture the membrane.

Fortunately, pressure measurements are fast, simple and cheap [27], with response times of less than 0.5 s. We will model the sensor and actuator as a simple delay, $\theta_{p_m} = 0.5$ s.

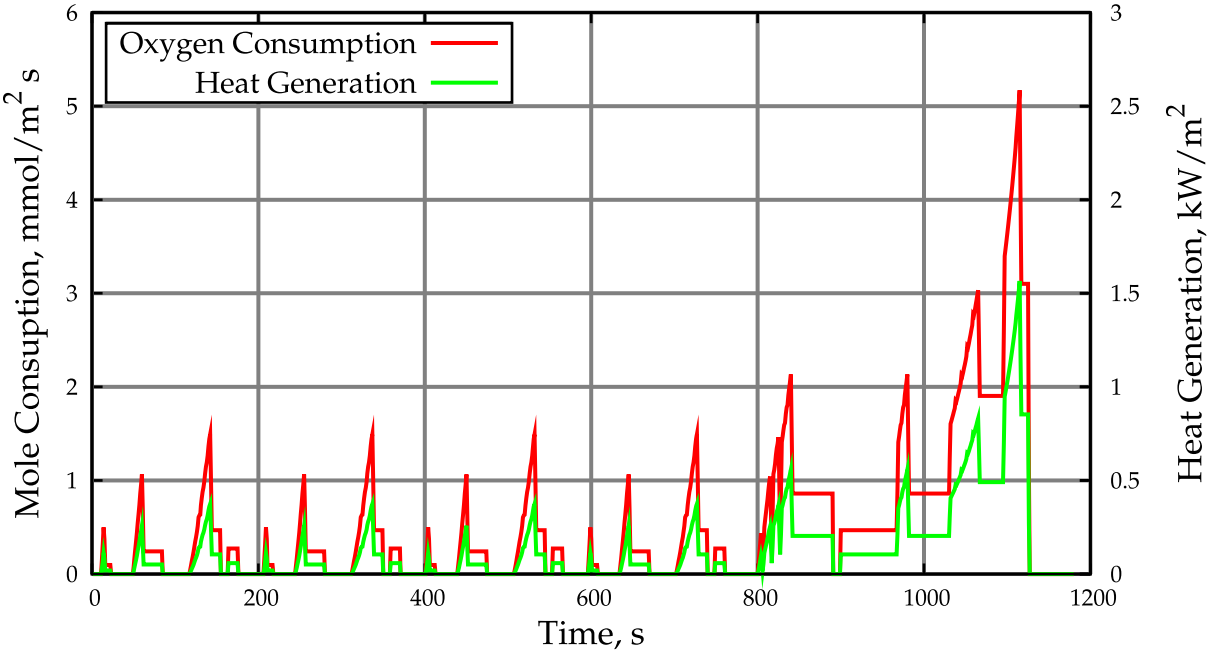

Fig. 7. The approximate plot of reactant consumption and heat generation along the entire NEDC cycle, assuming $X = 0$. As in practice X will be different from 0, real values could be slightly higher because of the increased overvoltage.

We define the PI control law as

$$u_{\text{feedback}} = \overbrace{K_{\text{P}}\left(\frac{\tau_{\text{I}}s+1}{\tau_{\text{I}}s}\right)}^{K(s)}(r - y_{\text{m}}) \tag{16}$$

where u is the manipulated variable, y_{m} is the measurement of the controlled variable (in this case p_{H_2}), and r the reference to be followed (in this case $p_{\text{H}_2}^{\text{ref}}$). For a PI controller, Skogestad [28] suggests the following settings:

$$\begin{aligned} K_{\text{P}} &= \frac{W}{RT}\frac{1}{\tau_{\text{c}}+\theta_{p_{\text{m}}}} \\ \tau_{\text{I}} &= 4(\tau_{\text{c}} + \theta_{p_{\text{m}}}) \end{aligned} \tag{17}$$

where the desired response time τ_{c} is the tuning parameter.

We can also add some feedforward action, since the only significant disturbance in the process, i_{r}, can be easily and rapidly measured

$$u_{\text{feedforward}} = K_{\text{ff}}\frac{i_{\text{r}}A}{2F} \tag{18}$$

Ideally, according to Eq. (15), parameter K_{ff} should be 1, but we may set a different value in simulations to represent the *implementation error*; this is necessary since the actual implementation of the controller will not be perfect, and feedforward control does not have the self-correcting behaviour that feedback has. Being able to assess how a real controller may behave in presence of implementation errors is therefore of greater importance.

When using both feedback and feedforward control, the molar inflow to be set is found by simply adding the two terms:

$$\dot{n}_{\text{H}_2} = u_{\text{feedback}} + u_{\text{feedforward}} \tag{19}$$

We assume $W = 30\ \text{m}^2 \times 1\ \text{mm} = 30\ \text{dm}^3$, where the area is the same we assumed above for the whole stack, and 1 mm is the thickness of a gas channel, as reported by Shan and Choe [23]. This neglects the manifold volume, and may therefore be a very low estimate: by Eq. (15), this will result in a significantly faster system: since the system is also unstable, being faster implies it will also be more difficult to control. Therefore, our low estimate of W is conservative in the sense that it represents the system most difficult to control.

To test the performance of this control strategy, we will simulate the effect of disturbance $i_{\text{r}}(t)$ as calculated previously for an NEDC cycle. We assume a constant temperature of 150 °C and use a set point $p_{\text{H}_2}^{\text{ref}} = 120$ kPa. The overall loop delay is set to $\theta_{p_{\text{m}}} = 0.5$ s.

In order to cope with input saturation and reduce input usage, τ_{c} was set by trial and error to a relatively large value, $\tau_{\text{c}} = 15$ s.

The parameters used in the modelling and control of the anodic pressure are summarised in Table 2.

5.4. Air-composition control (cathode)

Control of the partial pressure of oxygen at the cathode, the other reactant in the reaction, is not as simple as for hydrogen. Inert nitrogen and product water vapour cause diffusion limitations in the system.

To maintain a certain reaction rate, our main task is to maintain a minimum oxygen partial pressure (see also Section 4.2.1). Again, we assume that the inlet flow (air) can be manipulated directly; a more detailed approach could include a model for the blower or compressor used to drive the flow through the stack.

Table 2
The variables and parameters used in the dynamic model and control algorithm for anodic pressure

Symbol	Description	Value or role
p_{H_2}	Hydrogen pressure	Controlled variable
$p_{\text{H}_2}^{\text{ref}}$	Reference hydrogen pressure	Reference, 120 kPa
$\dot{n}_{\text{H}_2}$	Hydrogen molar inflow	Manipulated variable
i_{r}	Reaction current	Disturbance
T	Temperature	Disturbance
A	Anode area	30 m^2
W	Gas channel volume	30 dm^3
K_{P}	Proportional feedback constant	0.5502 mmol/s kPa at $T = 150$ °C
τ_{I}	Integral feedback constant	62 s
K_{ff}	Implementation error	1 (ideal controller)

Ensuring that the oxygen partial pressure in the cathode's bulk is acceptable is more challenging than controlling the hydrogen pressure. Oxygen's partial pressure is much more critical to the performance of the fuel cell than hydrogen's, because of the much higher overvoltage on the cathodic side. At the same time, composition measurements are slower than pressure measurements, resulting in less available bandwidth for feedback control.

The differential equation for the mole fraction of oxygen in a cell's cathode is a particular case of Eq. (9)

$$\frac{pW}{RT}\frac{\mathrm{d}x_{\mathrm{O}_2}}{\mathrm{d}t} = \dot{n}_{\mathrm{air}}\left(x^{\mathrm{in}}_{\mathrm{O}_2} - x_{\mathrm{O}_2}\right) - \frac{i_{\mathrm{r}}A}{4F}(1 + x_{\mathrm{O}_2}) \tag{20}$$

This equation presents the additional challenge of being nonlinear, but it has the advantage, compared to Eq. (15), of being stable: in the right-hand term, the coefficient of state variable x_{O_2} is always negative. This means that feedback is not strictly necessary, and a pure feedforward approach is possible.

5.4.1. Measurement dynamics

Measurement of oxygen concentration in gases is frequently reported to be very fast, with bandwidths in the range of 10 Hz [29], this is for off-gases from stacks or car exhausts where the temperatures are much higher than the ones we consider. Results more relevant for our temperature range (100–200 °C) were obtained by Yamamoto et al. [30], who reported that oxygen sensors operating at 100 °C reached steady state after about 3 min, under various values of composition; their plots indicate that the measurement dynamics operated roughly as a lag with a time constant of about 2 min. These lags may be reduced by purpose-built equipment, such as sensors that heat up samples of the stack's off-gases to high temperatures to make a faster measurement possible.

5.4.2. Actuator dynamics

A blower used to force air into the stack will have its own dynamics, which will limit the achievable control performance. Pukrushpan [14], in his PhD thesis, modelled a blower with a first-order dynamic system with a time constant of 0.3 s. Goldschmied and Wormley [31], who developed a more detailed model, claim that a blower will operate at quasi-steady conditions for frequencies below a variable threshold between 10 and 20 Hz (for the range of data they considered), increasing with flow.

5.4.3. Time constants of composition dynamics

The time constant[2] is defined by writing the differential equation in the form $\tau\frac{\mathrm{d}x}{\mathrm{d}t} = -x$. We find that the time constant is quite small:

$$\tau_{\mathrm{O}_2} = \frac{pW}{RT}\frac{1}{\dot{n}_{\mathrm{air}} + \frac{i_{\mathrm{r}}A}{4F}} \approx 9\ \mathrm{s} \tag{21}$$

Here we have assumed atmospheric pressure, $i_{\mathrm{r}} \approx 200\ \mathrm{A/m^2}$ (roughly the average value through the NEDC with our parameters), $\dot{n}_{\mathrm{air}} \approx 5 \times \frac{i_{\mathrm{r}}A}{4F}$ (since the air molar flow has to be about five times the oxygen flow), and all other conditions are as for the hydrogen manifold's case. This indicates that, once a certain input and disturbance are fixed, the system quickly approaches a steady state: this is especially beneficial for feedforward control, since feedforward techniques cannot change the system dynamics.

It should be remarked that volume W is, in this case, only the volume inside the gas channels, whereas in the case of pure hydrogen it was supposed to be all the volume after the control valve, including manifold and piping: that made $W = 30\ \mathrm{dm^3}$ a low estimate. The hydrogen manifold and piping after the control valve could be included because pressure is transmitted almost instantaneously across that whole volume, whereas diffusion occurs only in the gas channels, not in the whole air manifold. Therefore, in this case, we do not have the option of increasing the system's time constant by adding some gas buffer that would increase W, which we may have desired to do in order to slow down the process relatively to the control system (which includes the slow measurements), making conditions easier for feedback control.

5.4.4. Feedforward control

Since the system has satisfyingly fast time constants and is stable, we will consider pure feedforward control. In this case, feedforward control presents many advantages:

- it does not introduce instabilities;
- it does not rely on measurements of the system's state, which in this particular case are much slower than the system's own dynamics;
- it relies on a measurement of the system's only disturbance, i_{r}, which we can obtain inexpensively, with high precision and large bandwidth;
- in the overall layout sketched in Fig. 8, temperature control competes with this algorithm for the usage of air inflow as a manipulated variable. In these conditions, a PI controller for air composition could exhibit integral wind-up problems.

A feedforward controller cannot provide zero error at steady state (since feedforward has, by definition, no measurement of the error), but fortunately we are not concerned about precise tracking, but rather with maintaining an acceptable value of x_{O_2} to guarantee the stack's capability to produce the desired power output.

We may therefore consider setting $\dot{n}_{\mathrm{air}}$ so that it compensates for the effects of i_{r} in Eq. (20), ideally making its right-hand term zero. A feedforward control law is then

$$\dot{n}_{\mathrm{air}} = \frac{K_{\mathrm{ff}}}{1 + \tau_{\mathrm{a}}s}\frac{i_{\mathrm{r}}A}{4F}\frac{1 + x^{\mathrm{ref}}_{\mathrm{O}_2}}{x^{\mathrm{in}}_{\mathrm{O}_2} - x^{\mathrm{ref}}_{\mathrm{O}_2}} \tag{22}$$

where K_{ff} is again the implementation error, and τ_{a} is the actuator lag representing the dynamics of the blower or compressor.

The variables and parameters used in the modelling of the dynamics of oxygen fraction and its control are summarised in Table 3.

5.5. Temperature control

The temperature needs to be kept within certain boundaries. It is very common in Nafion-based cells to have a separate cooling loop to take care of heat removal [1]; this is necessary because the low-temperature operation does not allow the released heat to be dissipated by the exiting flows alone. However, this cooling system requires channels integrated in the bipolar plates of the stack, which are the most expensive components in fuel cell systems [1], adding to their cost and complicating the design.

This paper will investigate the possibility of avoiding this additional cooling system, using the air flow to indirectly cool the stack. This is possible because of the high temperatures of PBI fuel cells implies that much more heat is transported in the exhaust gas.

Obviously, there is an issue of not having enough degrees of freedom because we want to use air flow to control both oxygen partial pressure and stack temperature. However, the requirement on air-composition control is only a minimum one: an oxygen concentration higher than specified will not be harmful. Thus, we can use the air flow to control temperature, as long as it remains above the threshold required by air-composition control.

[2] Since the system is nonlinear, the time "constants" are in fact quite variable.

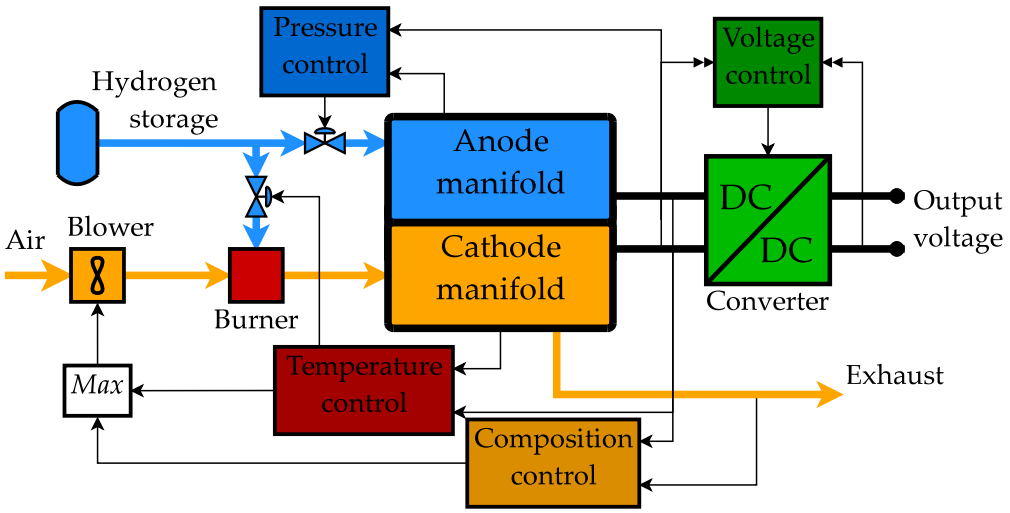

Fig. 8. The suggested layout for control of a PBI fuel cell stack, with four independent control loops.

Table 3
The variables and parameters used in the dynamic model and control algorithm for cathodic oxygen fraction

Symbol	Description	Value or role
x_{O_2}	Oxygen fraction	Controlled variable
$x_{O_2}^{ref}$	Reference oxygen fraction	Reference, 0.15
$\dot{n}_{air}$	Air molar inflow	Manipulated variable
i_r	Reaction current	Disturbance
T	Temperature	Disturbance
p	Atmospheric pressure	101 325 Pa
A	Cathode area	30 m^2
W	Gas channel volume	30 dm^3
$x_{O_2}^{in}$	Oxygen fraction in air	0.2
K_{ff}	Implementation error	1 (ideal controller)
τ_a	Actuator lag	0 (ideal actuator)

When the stack requires heating rather than cooling, for example at start-up, it is possible to burn some hydrogen at the cathode inlet, to increase its temperature. The possibility of just shorting the stack in these conditions to use reaction heat would not work, because the reason we require a start-up procedure is exactly that the maximum reaction rate is limited. A slightly more complex approach would be to implement a heat exchanger between the air inlet and outlet, but we will consider only the former approach in this paper.

The objective of temperature control is to keep the stack at a given temperature by manipulating the air flow. Having assumed that temperature is uniform in a stack, its dynamics is determined by Eq. (10). However, in that form the equation has some flaws:

- calculating the entering enthalpy requires making assumptions on the control algorithm for the anode flow (not for the cathode flow, which is our manipulated variable);
- calculating the exiting enthalpy requires tracking a set of differential equations for all involved species. This is not difficult to simulate, but we would prefer a simpler model for controller synthesis.

For control synthesis purposes, we will further simplify the model so that flow dynamics do not interfere with temperature dynamics. We will assume that:

- the anode (hydrogen) flow is under perfect control, so that $\dot{n}_{H_2} \equiv \frac{i_r A}{2F}$;
- there is no composition transient in the cathode (air) flow.

In practice we are assuming a condition of pseudo-steady state, discarding all dynamic modes but the temperature's. The energy balance can now be translated into a more manageable form, splitting the enthalpy difference in two parts, one for reaction heat and one for sensible heat:

$$\begin{aligned} A\hat{c}_p \frac{dT}{dt} &= \dot{H}^{in}(T^{in}) - \dot{H}^{out}(T) - i_r VA \\ &= \overbrace{\left(\dot{H}^{in}(T) - \dot{H}^{out}(T)\right)}^{\text{Reaction heat}} - \overbrace{\left(\dot{H}^{in}(T) - \dot{H}^{in}(T^{in})\right)}^{\text{Sensible heat}} - i_r VA \\ &\approx \overbrace{-\Delta h_r(T)}^{\approx 243\ \text{kJ/mol}} \left(\frac{i_r A}{2F} + \dot{n}^c_{H_2}\right) - \sum_i c_{p,i}\dot{n}^{in}_i (T - T^{in}) - i_r VA \end{aligned} \tag{23}$$

In the last line of the equation we assumed that constant-pressure specific heat for all the species is approximately constant: this is not very accurate, but for control-oriented modelling we are more interested in a good approximation than in an accurate model. We also implicitly assumed that any hydrogen sent to the cathode inlet ($\dot{n}^c_{H_2}$) is completely consumed.

We can now express the temperature dynamics in the following approximate form, which lends itself well to control synthesis:

$$\begin{aligned} A\hat{c}_p \frac{dT}{dt} \approx & -c_{p,air}(T - T^{in})\dot{n}_{air} - \left(\Delta h_r(T) + c_{p,H_2}(T - T^{in})\right)\dot{n}^c_{H_2} \\ & + -\left(\frac{\Delta h_r(T) + c_{p,H_2}(T - T^{in})}{2F} + V\right) A i_r \end{aligned} \tag{24}$$

The equation may be simplified further, noting that $c_{p,H_2}(T - T^{in})$ is much smaller than the enthalpy of reaction:

$$\begin{aligned} A\hat{c}_p \frac{dT}{dt} \approx & -c_{p,air}(T - T^{in})\dot{n}_{air} \overbrace{-\Delta h_r(T)}^{\approx 243\ \text{kJ/mol}} \dot{n}^c_{H_2} \\ & + \left(\overbrace{-\frac{\Delta h_r(T)}{2F}}^{\approx 1.26\ \text{V}} - V\right) A i_r \end{aligned} \tag{25}$$

Our system is unfortunately nonlinear in the main manipulated variable, $\dot{n}_{air}$. On the other hand, the system is stable (as long as $T > T^{in}$): as in the case of cathodic composition, we could rely on feedforward control only. However, as this model contains many more approximations, the effects of disturbance i_r could deviate markedly from the ones predicted by Eq. (25), or will require a more difficult

calculation to be estimated. We have also discarded any effect of heat loss to the environment, meaning that the performance of a pure feedforward approach will be less predictable. This inaccuracy of the model makes a feedback controller more interesting.

5.5.1. Reference for temperature control

Unfortunately, it is not yet clear how to determine the temperature at which a PBI fuel cell stack should operate at a particular time. On one hand, high temperatures improve reaction rate, tolerance to poisons such as CO and membrane conductivity, but on the other hand they increase the stack's heat losses, reduce the membrane's mechanical strength and could accelerate the decay of its properties.

Until precise models of the overall effects of temperature on PBI fuel cells appear in the open literature, it will not be possible to synthesise a sound criterion to determine the best temperature at which the stack should be kept.

As determining an optimal operating temperature is beyond the scope of this paper, we will simply assume that a reference has somehow been decided, and we will concentrate on the controller instead.

5.5.2. Hydrogen in the cathodic flow as an input variable

When using $\dot{n}^{c}_{H_2}$ as a manipulated variable to raise the temperature of the entering cathodic flow, there is a danger of raising the temperature so much that the membrane or other components in the fuel cell stack could be damaged. It is therefore necessary to define a maximum input level beyond which control action will be ignored. A reasonable criterion may be to limit entering temperatures to $T^{max} = 200\,^{\circ}C$: in that case, the energy balance yields

$$\left(c_{p,air}\dot{n}_{air} + c_{p,H_2}\dot{n}^{c}_{H_2}\right)(T^{max} - T^{in}) \approx -\Delta h_r \dot{n}^{c}_{H_2} \tag{26}$$

This simplified equation has been obtained by equating the increase in sensible heat in the flow to the reaction heat of hydrogen, assuming all hydrogen is consumed; we have again approximated using constant specific heats. The resulting saturation condition is

$$\dot{n}^{c}_{H_2} < \frac{c_{p,air}(T^{max} - T^{in})}{-\Delta h_r - c_{p,H_2}(T^{max} - T^{in})}\dot{n}_{air} \approx \frac{c_{p,air}(T^{max} - T^{in})}{-\Delta h_r}\dot{n}_{air} \tag{27}$$

In the last term in the previous equation we neglected the heating of hydrogen, as it is negligible compared to the reaction heat: the resulting simplified condition is both conservative and linear in T^{max}. An approximate value for the limit of the hydrogen flow burnt to pre-heat the entering cathode gases is about $2\%_{mol}$ of the air flow.

5.5.3. Measurement dynamics

According to Cimerman et al. [32], temperature-measurement dynamics shows a certain dependence on pressure and gas velocity, with the dominant time constants being in the range of 10–100 s. Whereas pressure at the outlet of the cell stack will be fairly constant at atmospheric value, gas velocity could change significantly depending on the current gas inflow, and to some degree on the reaction rate. Furthermore, if the temperature measurement is placed at the stack's outlet, a delay in measurement will occur because of the time outlet gases use to pass through the exit manifold. We will assume a worst-case condition with a lag $\tau_{T_m} = 100$ s and a delay $\theta_{T_m} = 10$s.

5.5.4. Time constants of temperature dynamics

As for the case of composition control, it is useful to estimate the system's time constants. As $\Delta h_r(T)$ does not change significantly with temperature, terms related to it (i_r and $\dot{n}^{c}_{H_2}$) will be ignored. The time constants are derived from Eq. (23):

$$\tau_T \approx \frac{A\hat{c}_p}{\sum_i c_{p,i}\dot{n}_i} \approx 19000\ \text{s} \tag{28}$$

In this expression, we assumed for approximation that the gases' specific heats are all 29 J/mol K, that hydrogen flow is stoichiometric and that air flow is perfectly controlled to maintain an oxygen fraction of 0.15 in the cathode gases. Since the average current density through the NEDC cycle is 200 A/m^2, this results in an average value $\sum_i \dot{n}_i = (1 + \frac{1+0.15}{0.2-0.15})\frac{i_r A}{4F} \approx 373$ mmol/s. This time constant corresponds to over 5 h, but can be made significantly smaller by increasing the air flow, and with it the stoichiometric ratio.

Indeed, if we set $\dot{n}_{air}$ such as to balance out the approximate differential equation (25), knowing that the average power density output through the NEDC cycle is $Vi_r \approx 120$ W/m^2, and assuming a temperature difference $T - T^{in} \approx 150$ K, we obtain a much larger flow:

$$\dot{n}_{air} = \frac{\frac{-\Delta h_r}{2F}Ai_r - Vi_r A}{c_{p,air}(T - T^{in})} \approx 910\ \text{mmol/s} \tag{29}$$

This will result in specularly smaller time constants (in this specific example, about 2 h).

5.5.5. Controller synthesis

We have seen that, fortunately, the time constants of temperature dynamics are much slower than temperature measurements, with a gap of about two orders of magnitude. To devise an appropriate controller, we use again Skogestad's tuning rules (Eq. (17)); to avoid a too aggressive controller that could saturate the input variable (we cannot have $\dot{n}_{air} < 0$), we set a large desired response time, $\tau_c \approx 100$ s.

As previously remarked, the system in Eq. (25) is stable but nonlinear. In order to apply linear control theory, we first have to change the control variables so that the system becomes linear. It is straightforward to define the input variable as

$$u = -c_{p,air}(T - T^{in})\dot{n}_{air} - \Delta h_r(T)\dot{n}^{c}_{H_2} \tag{30}$$

It would then be possible to control the system using u, calculating back the value of $\dot{n}_{air}$ (or if necessary $\dot{n}^{c}_{H_2}$) to apply when setting the actuator. However, this transformation has made the system unstable[3]: it is now an integrating process, and will require feedback to be stabilised. The ultimate cause of the induced instability is the form of actuator function $\dot{n}_{air} = f(u)$, which depends on a temperature measurement: to remove this internal feedback and make the system stable again, we use the reference T^{ref} directly, instead of temperature T.

We proceed then to synthesise a feedback controller. Since control variable $\dot{n}_{air}$ is set to be the maximum of the signals coming from the control loops of composition and temperature, using a temperature controller containing an integrator could cause wind-up issues. Therefore, we will use a simple proportional controller. The feedback control law is then

$$\dot{n}_{air,\,feedback} = K_P(T^{ref} - T_m) \tag{31}$$

$$K_P = -\frac{A\hat{c}_p}{c_{p,air}(T^{ref} - T^{in})}\frac{1}{\tau_c + \theta_{T_m}} \tag{32}$$

We also add a feedforward term to improve the dynamic properties of the controller:

[3] In fact, the system is still stable: the heat loss $\dot{H}^{loss}$, which we neglected, will most likely increase with temperature. We also neglected the sensible heat necessary to heat hydrogen up to cell temperature, which will also have a stabilising effect on temperature. However, these contributions are small and will have little effect on dynamics.

$$\dot{n}_{\text{air, feedforward}} = K_{\text{ff}} \frac{\left(-\frac{\Delta h_{\text{r}}}{2F} - V\right) i_{\text{r}} A}{c_{p,\text{air}}(T^{\text{ref}} - T^{\text{in}})} \tag{33}$$

We will finally assume that the competing feedforward controller for air composition, developed in the previous section, is assumed to be perfectly implemented and set to $x_{O_2}^{\text{ref}} = 0.15$. Ambient temperature T^{in} is assumed to be 300 K, the stack's initial temperature 400 K, and reference T^{ref} is given constant at 450 K.

5.5.6. Temperature control with hydrogen combustion

Burning hydrogen in the cathode inlet to increase the inflow air temperature is a last resort to raise the stack's temperature when the stack itself cannot generate heat, typically because it is at too low a temperature for the electrochemical reaction to proceed and generate enough heat by itself. In that case, we also want to limit the inlet temperature so that the cells will not be damaged by excessive temperatures: this may be achieved by limiting the hydrogen flow into the cathode inlet's burner to $2\%_{\text{mol}}$ of the air flow.

However, it is also necessary to change the control strategy. The previously illustrated feedback and feedforward controllers were designed to increase temperature in the stack by maintaining a minimum air flow, which was set according to the requirements of the composition controller. When burning hydrogen in the cathode inlet, the entering air flow will actually have a temperature higher than the stack, so increasing flow will increase the stack's temperature, not reduce it as in the normal case.

As a possible start-up approach, we will consider a very simple strategy. When the stack temperature is measured to be lower than a preset minimum, in our example 400 K, cathodic stack inflow will be set to maximum, and hydrogen burnt in the entering cathode flow will be exactly 2% of that. The temperature at which the previously defined feedback and feedforward controllers take over should be below any operational value for temperature, to avoid hysteresis between the two modes. However, this temperature should also be high enough for the cell to be able to function and generate heat by itself.

As burning hydrogen on the cathode inlet is a wasteful usage of the available exergy of hydrogen, we should seek to reduce it as much as possible. It may be found advantageous to add a recuperating heat exchanger to pass heat from the cathode's outlet to the inlet to the burner. In this case, the hydrogen flow will also have to be carefully adjusted so that the temperature of entering air does not exceed the specified limits. Such a recuperating heat exchanger could also be useful when raising stack temperature, or when trying to maintain temperature at high flow rates (possibly caused by a high set point for $x_{O_2}^{\text{ref}}$). This exchanger will however be bypassed during normal operation, as it would only hinder the dissipation of reaction heat. The variables and parameters used in the simulation and control of the temperature dynamics are summarised in Table 4.

5.6. Summary of the control strategy

In this section, we have developed a series of simple controllers for each of the dynamic modes we want to control.

The overall control layout is in Fig. 8 with the four control loops for power (or voltage), hydrogen pressure, temperature and oxygen concentration.

- Hydrogen pressure in the anode is controlled by a controller with a PI feedback and a feedforward component, using measurements of hydrogen pressure and cell current, with hydrogen inflow as the input.
- Oxygen concentration in the cathode is controlled with a feedforward controller, using a measurement of cell current and manipulating the air inflow.

Table 4
The variables and parameters used in the dynamic model and control algorithm for stack temperature

Symbol	Description	Value or role
T	Temperature	Controlled variable
T^{ref}	Reference temperature	Reference, 450 K
T_{m}	Measured temperature	Measurement
$\dot{n}_{\text{air}}$	Air molar inflow	Manipulated variable
$\dot{n}_{H_2}^{\text{c}}$	Hydrogen inflow	Manipulated variable
i_{r}	Reaction current	Disturbance
V	Stack voltage	Disturbance
$T^{\max}$	Maximum inlet temperature	200 °C
T^{in}	Ambient temperature	300 K
A	Anode area	30 m^2
Δh_{r}	Reaction heat	≈−243 kJ/mol
$\tilde{c}_p$	Areal heat capacity of the stack	7 kJ/mol K
$c_{p,\text{air}}$	specific heat capacity of air	≈29 J/mol K
K_{P}	Proportional feedback constant	−0.439 mol/s K
K_{ff}	Feedforward implementation error	1 (ideal controller)

- Temperature is controlled with a P feedback controller, optionally with a feedforward component as well that uses current and voltage as measurements, and manipulates the air inflow.
- The air inflow, which is the input variable for the last two controllers, is set by selecting the maximum value required from these, since oxygen concentration cannot be allowed to fall below a threshold, but can be any value higher than that.
- At start-up, when heating is required, hydrogen will be burnt directly into the cathode inlet; a simple feedforward strategy, using a fixed ratio of hydrogen versus inlet air, has been proposed.

6. Results

After the analysis of the dynamics of the model and the control synthesis performed in the previous chapters, it is possible to visualise the time scales of the various dynamic modes in Fig. 9. Note that hydrogen pressure, being an integrating process, does not have time constants; the bandwidth of the PI controller has been used.

6.1. Hydrogen pressure control

The simulation results for one NEDC cycle are plotted in Fig. 10. The simulation for the case of feedback-only control results in a negative pressure; in a real application, the fuel cell would simply have run out of fuel at a pressure close to zero, and the reaction rate would have been brought to a halt. The combination of feedback and feedforward has also been included, assuming implementation errors of ±20%.

6.2. Oxygen composition control

The air-composition control strategy's performance through an NEDC cycle is plotted in Fig. 11. The control law of Eq. (22) takes full advantage of the relatively fast dynamics of x_{O_2}, and maintains an acceptable approximation of the set point even with a large implementation error, −20%[4]. When adding a significant actuator lag (1 s), some oscillations do appear, yet operation is not significantly disturbed.

[4] We did not consider the case of a positive implementation error, as we are concerned only with having too little oxygen: excess oxygen will not cause problems, even if the overall efficiency of the system could suffer because of increased input usage.

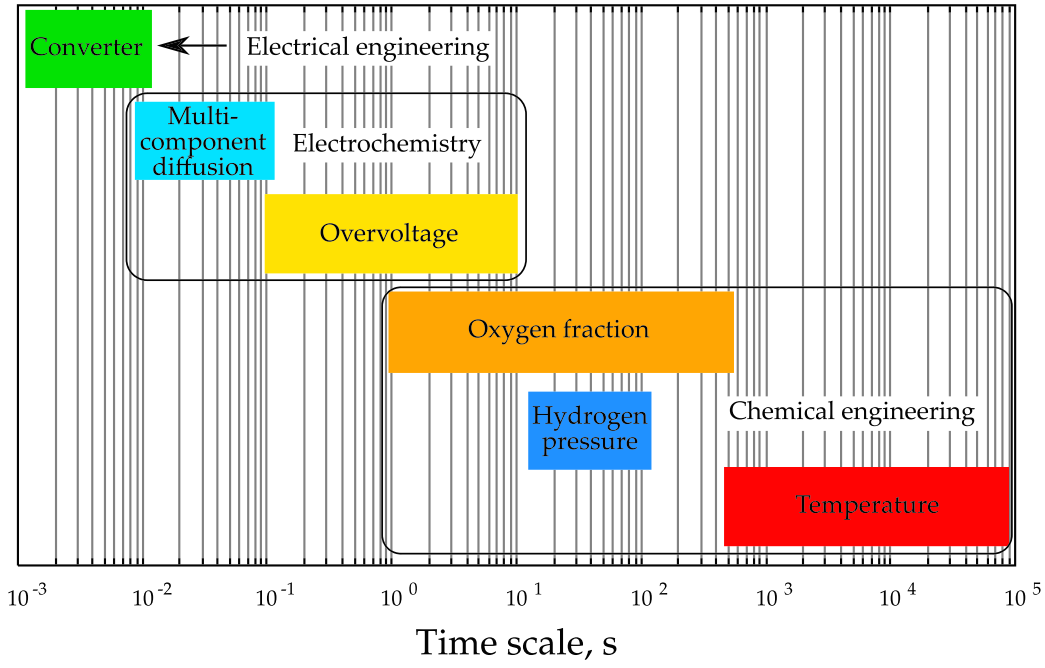

Fig. 9. Summary of the time scales of the various dynamic modes of PBI fuel cells.

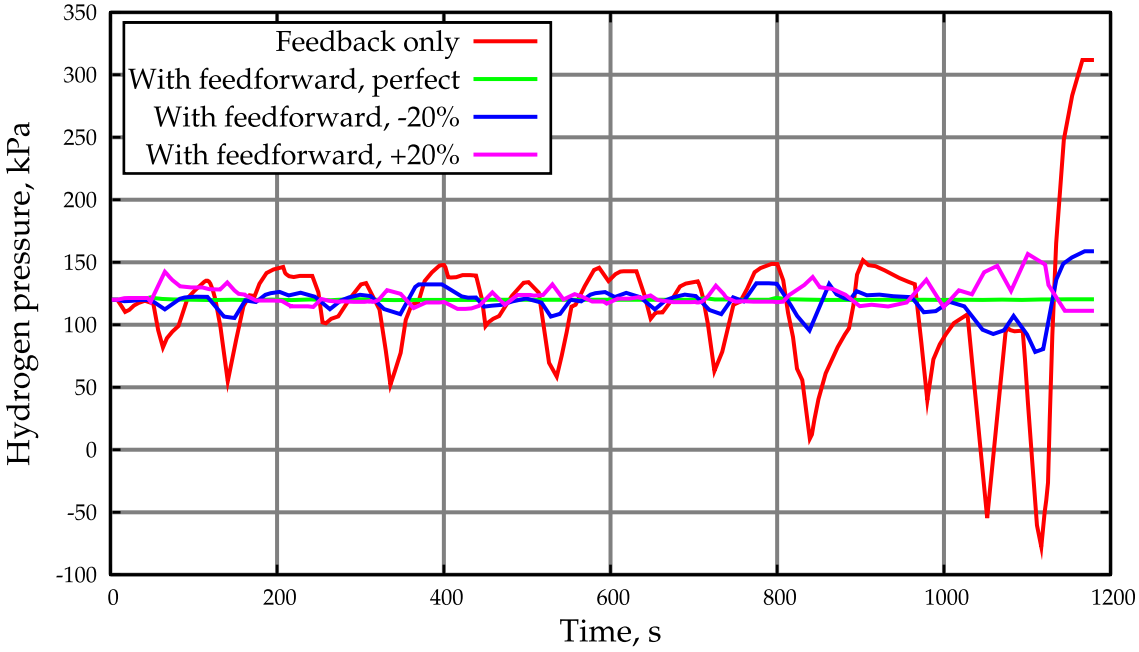

Fig. 10. Control of hydrogen pressure during an NEDC cycle.

6.3. Temperature control

The proposed control structure for temperature has been simulated against the original thermal model of Eq. (10), which also includes the transients in composition of all cathodic species. The results, for the cases of feedback-only and feedback with feedforward, are plotted in Fig. 12 for a series of 10 NEDC cycles. The air flow required for our test case is plotted in Fig. 13 for the case of feedback only and for the case with feedforward as well; no gain errors in either composition or temperature control are modelled.

The effects of the set point for oxygen molar fraction are pictured in Fig. 14. The feedback–feedforward approach of Fig. 12 (this time with no feedforward gain error) has been put in competition with feedforward composition controllers with increasing set points.

For the simulation of a stack start-up with hydrogen combustion, temperature as a function of time is plotted in Fig. 15, where hydrogen is fed to the cathode inlet burner for 1160 s; hydrogen burning continues for some time after reaching 400 K because of the lag and delay in temperature measurement, which determines burner usage. With the assumed maximum flow, it will take about

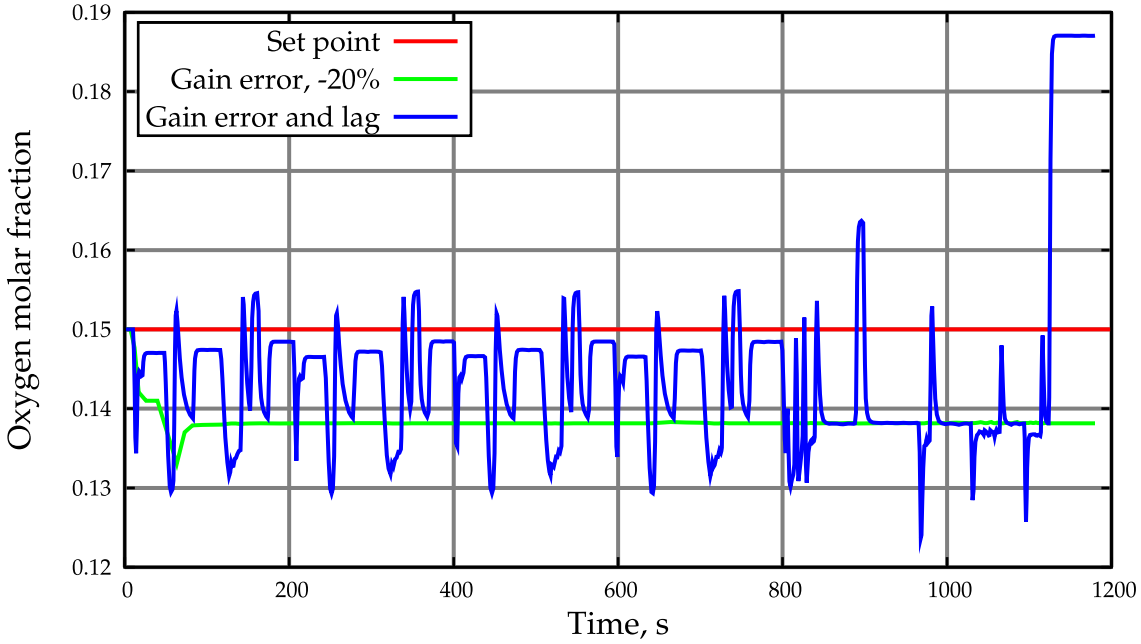

Fig. 11. Feedforward control of oxygen concentration during a NEDC cycle. The implementation error is −20 % and the actuator lag 1 s.

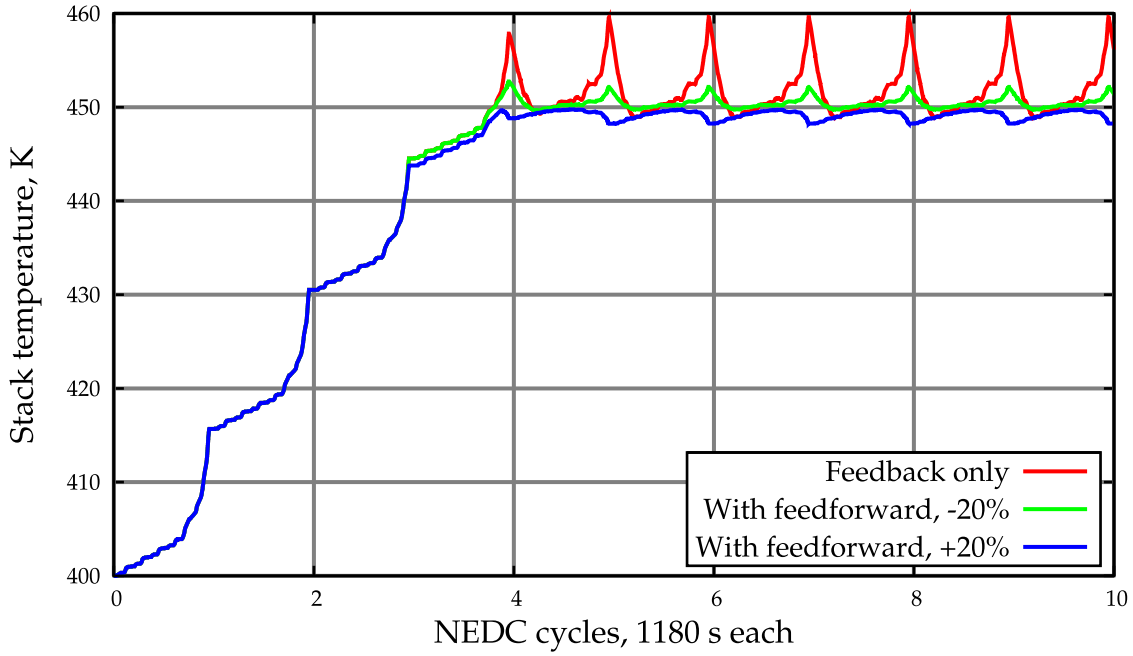

Fig. 12. Control of temperature during 10 NEDC cycles. In the first four NEDC cycles temperature control is overridden by composition control.

the duration of an entire NEDC cycle to heat up the stack to the minimum functioning temperature.

7. Discussion

7.1. Hydrogen pressure control

In the case of anodic pressure control, Fig. 10 indicates that feedback alone is insufficient, as pressure reaches negative values in the simulation. To improve performance, feedforward proved necessary. Even in the case of large implementation errors (±20%), feedforward made control performance acceptable.

It is not possible to discard the feedback loop and adopt a purely feedforward approach, as system (15) is unstable and requires feedback for stabilisation.

It is possible to make the feedback loop more controllable, and possibly sufficient to control the process without the assistance of feedforward, by increasing volume W so that hydrogen pressure will change more slowly.

7.2. Oxygen composition control

The feedforward-only control law proposed for air-composition control has shown excellent results in Fig. 11. One of the reasons

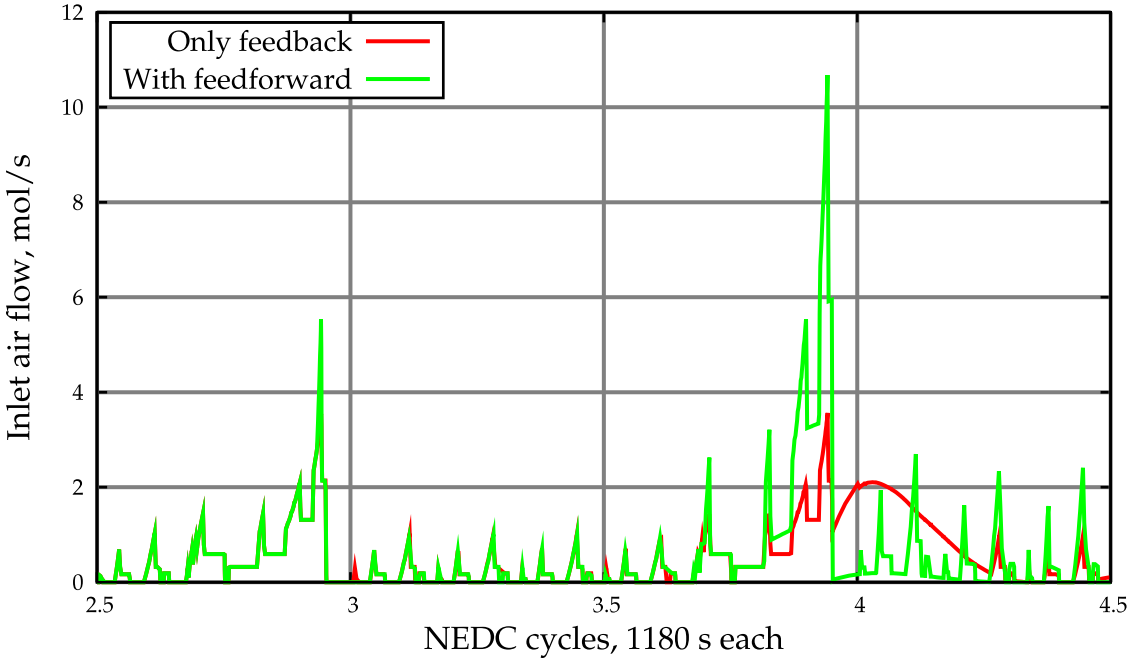

Fig. 13. Use of the manipulated variable (air flow) by the joint composition-temperature control system of Fig. 8, connected by a maximum selector. The first peak is determined by composition control, the second by temperature control. For clarity, only a fraction of the simulation is shown.

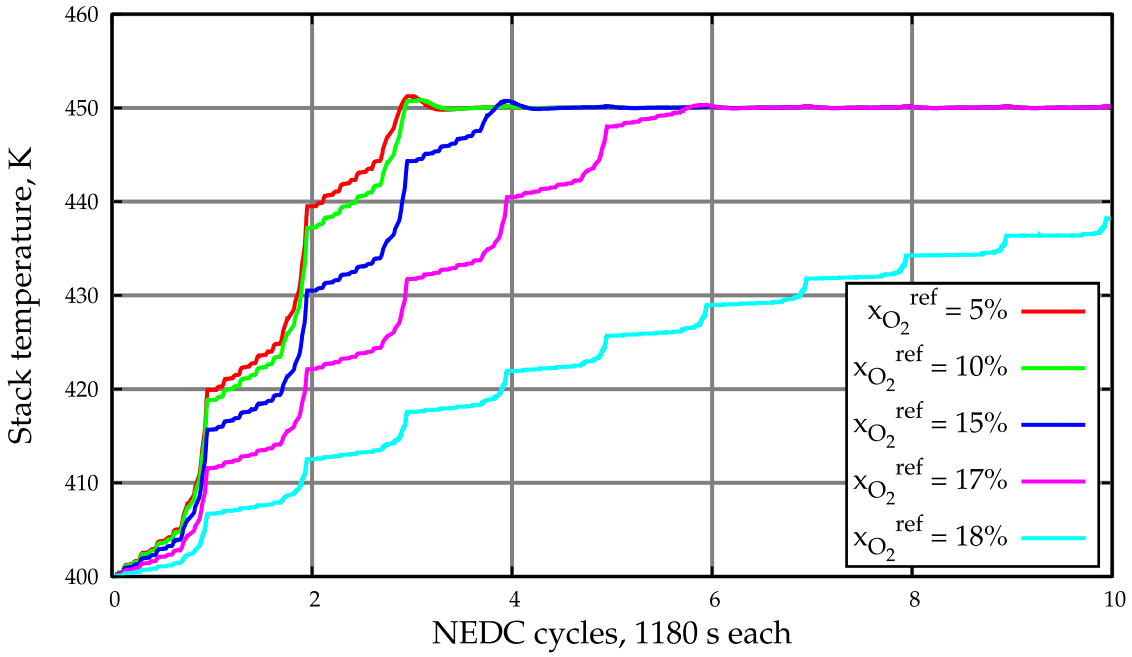

Fig. 14. The influence of the set point for composition control on the performance of temperature control. All feedforward controllers, both for composition and temperature control, are modelled without gain error.

why feedforward works so well is that the system stabilises itself faster when there is a larger disturbance: the system's time constants (Eq. (21)) are much faster for high values of i_r, resulting in much faster dynamics right when the disturbance is at its strongest.

To apply the proposed feedforward control strategy, it is necessary to provide a value for $x_{O_2}^{ref}$. Ideally we would want this to be as high as possible in order to maximise the maximum allowable current, but we cannot simply set $x_{O_2}^{ref} = x_{O_2}^{in}$: it would make input usage infinite (Eq. (22)). Indeed, an excessive setting will reduce the system's overall efficiency because of the power losses in the actuator.

We can establish a simple criterion for an acceptable value of $x_{O_2}^{ref}$: it should be the value at which the marginal increase in maximum power output from the fuel cell equals the marginal increase in power lost to the blower. The actual value of this set point will however depend on the particular characteristics of the actuator and of the flow resistance of the stack, and cannot be established in general.

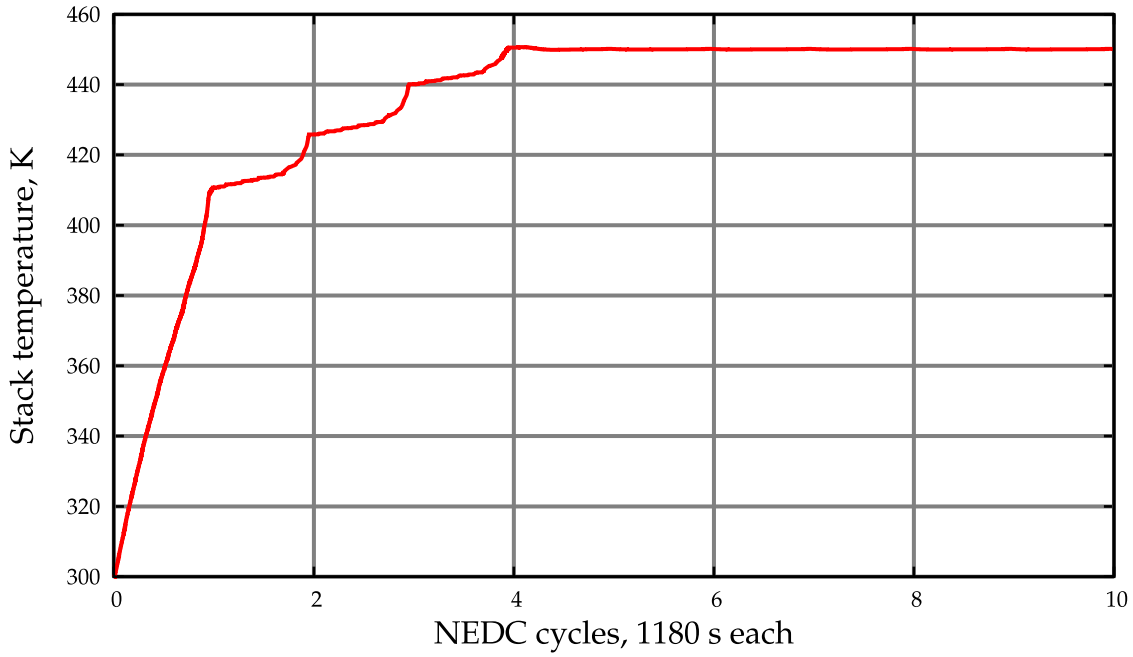

Fig. 15. The start-up from ambient temperature of a fuel-cell stack. The burner is active until the stack is measured to reach 400 K (note the measurement lag).

This criterion for oxygen concentration can be translated to a dimensioning criterion for the stack: the maximum available power from the stack will be the one obtained from the power density curve in Fig. 5 for the conversion corresponding to $x_{O_2}^{ref}$. We can therefore calculate the total area that we need to produce a given power. This maximum power density will always be less than that obtained for $x_{O_2}^{in}$, which is the one usually measured under laboratory conditions and reported in the literature.

7.3. Temperature control

Even with the many simplifications introduced in controller design, the resulting feedback controller is able to maintain the stack within 10 K of its set point, with peaks corresponding to the stack's maximum power outputs in the NEDC cycles. The addition of a feedforward component, even with a large ±20% gain error, manages to keep the oscillations in a narrow band of just 5 K. However, the slow dynamics of stack temperature still require about four NEDC cycles (about one hour and fifteen minutes) to reach 450 K from the starting temperature of 400 K: during this time, the temperature controller tries to keep the lowest possible air feed rate, and is superseded by the air composition controller. Using a higher setting for $x_{O_2}^{ref}$ will result in a higher minimum air flow, and therefore longer transient time when stepping up the temperature reference.

The most important observation from Fig. 13, representing the required air flow for temperature control, is that the air flow required to control the stack's temperature is not impractically higher than the one required to maintain the reaction, and is indeed not higher at all for the case of feedback control only: the first three NEDC cycles are dominated by the air-composition controller, which is at that time setting the lower bound of air flow (as shown in Fig. 12), whereas the later ones are caused by the feedforward component of temperature control.

The peaks in the air flow required by composition control must actually be strictly followed, because otherwise the fast composition dynamics at high currents would rapidly deplete the oxygen supply, and thereby halt the stack's operation. Instead, the slower dynamics of temperature allows a significant relaxation of the peaks requested by feedforward temperature control, possibly by using a low-pass filter on the feedforward component or by discarding it entirely: the stack temperature could temporarily increase, as it does under feedback control, but this will not disrupt operation of the stack, whereas oxygen depletion would immediately halt the reaction current. The heat is then dispersed by maintaining a lower peak air flow over a longer time.

As the air composition requirement increases beyond 15%, temperature dynamics rapidly deteriorate. At some setting of $x_{O_2}^{ref}$, increasing or maintaining temperature will eventually become impossible, because of the excessive requirements of composition control: this places an upper boundary on the value of $x_{O_2}^{ref}$, beyond which temperature control is infeasible. It is possible, if desired, to push this boundary by adding a recuperating heat exchanger between the cathode outlet and inlet, to maintain heat in the system.

The composition set point, however, influences the performance of temperature control only for the case of increasing stack temperature, when composition control requires higher minimum thresholds to maintain a certain composition: since composition control does not set a *maximum* threshold, the temperature control loop will not be limited by it when the objective is to decrease the stack temperature, and it will be able to set an air flow as high as feasible for the actuator.

The rise time of temperature in a cold stack, shown in Fig. 15, may be reduced by increasing the maximum flow during the start-up sequence, which could require modifications to the stack and its ancillary units. As the ratio of hydrogen and air is fixed, the specific enthalpy of the entering flow is constant with respect to the air flow[5]: this means that the rise time to the minimum operating temperature will be roughly inversely proportional to the maximum air flow the blower or compressor can produce. The design start-up time will therefore set a requirement on the actuator dimensioning.

[5] Assuming no significant contribution from the blower or compressor.

Table 5
The set of controllers proposed in this article to control the dynamic modes related to chemical engineering of a PBI-membrane fuel cell

Controlled variable	Controller type	Manipulated variable
Hydrogen pressure	PI feedback and feedforward	Hydrogen inflow
Oxygen fraction	Feedforward	Air inflow
Temperature	P feedback, optionally with feedforward	Air inflow
Temperature (start-up)	Feedforward	Air inflow and hydrogen burning

8. Conclusions

This article has tried to present a complete view of the dynamics of a particular type of high-temperature PEM fuel cell, and the control systems that would be needed to permit its operation.

It is important to realise that fuel cells have many dynamic modes, as illustrated by Fig. 1. These influence each other, but operate in different time scales, as summarised in Fig. 9.

Even if some dynamic modes are very slow, such as temperature's, this is not necessarily a relevant factor in determining the overall control performance. In fact, this depends very much on how we define performance.

If we were to define the control performance in terms of the temperature transient, we may come to the conclusion that fuel cells are very slow systems; if we considered only oxygen concentration, we would conclude that application of feedback control is impractical due to the large delays in measurement.

However, most users would define the performance of a fuel cell system according to the dynamics of its intended task, namely to deliver electric power. This has been shown not to be limited by the overvoltage transient [5], but only by the converter dynamics [6]. Once these are controlled, they define the performance of the system, as far as a user is concerned.

Yet, other dynamic modes cannot simply be ignored: the main objective for the three control loops related to chemical engineering (stack temperature, cathodic oxygen fraction, anodic hydrogen pressure) is to maintain acceptable conditions for the reaction to be possible. However, their dynamic requirements are not as stringent as for power production.

The results presented in the previous sections are summarised in Table 5.

8.1. Further work

This article considered a small subset of fuel cells. It would be useful to develop control strategies for Nafion-membrane PEM fuel cells, where water management must be taken into account, or solid-oxide fuel cells, which have radically different structure, reactions and purpose.

Even for the polybenzimidazole membranes considered in this article, data is lacking. It would be of particular interest to implement data regarding anodic resistance to CO poisoning, membrane conductivity as a function of temperature and humidity, and membrane degradation to obtain a reasonable set point for temperature.

The dynamics of hydrogen storage and supply have not been considered in this article, but will be of great importance in the actual performance of a fuel cell system. It would be useful to model the dynamics of various types of hydrogen storage, such as gas tanks, cryogenic storage, or metal hydrides.

PBI fuel cells are particularly apt to utilise hydrogen produced by steam reforming, due to their tolerance for CO. The presented model could be extended for the case of an open-end anodic manifold, which is necessary to avoid accumulation of poisoning species.

The lumped-parameter model presented in this paper cannot account for a non-uniform distribution of the reactant flows and of temperature gradients in the stack. Future models may simulate a number of cells with potentially different inflows and temperatures.

References

[1] James Larminie, Andrew Dicks, Fuel Cell Systems Explained, first ed., Wiley, 1999.
[2] Claire H. Woo, Jay B. Benziger, PEM fuel cell current regulation by fuel feed control, Chemical Engineering Science 62 (2007) 957–968.
[3] Keith A. Williams, Warren T. Keith, Michael J. Marcel, Timothy A. Haskew, W. Steve Shepard, Beth A. Todd, Experimental investigation of fuel cell dynamic response and control, Journal of Power Sources 163 (2007) 971–985.
[4] Jianlu Zhang, Zhong Xie, Jiujun Zhang, Yanghua Tang, Chaojie Song, Titichai Navessin, Zhiqing Shi, Datong Song, Haijiang Wang, David P. Wilkinson, Zhong-Sheng Liu, Steven Holdcroft, High temperature PEM fuel cells, Journal of Power Sources 160 (2006) 872–891.
[5] Federico Zenith, Frode Seland, Ole Edvard Kongstein, Børre Børresen, Reidar Tunold, Sigurd Skogestad, Control-oriented modelling and experimental study of the transient response of a high-temperature polymer fuel cell, Journal of Power Sources 162 (1) (2006) 215–227.
[6] Federico Zenith, Sigurd Skogestad, Control of fuel-cell power output, Journal of Process Control 17 (2007) 333–347.
[7] US Army Electronics Command, 22nd Annual Power Sources Conference, Atlantic City, NJ, May 1968.
[8] P.G.P. Ang, H.H. Ewe, E.W. Justi, A.W. Kalberlah, A simple miniaturized methanol-feed control for fuel cells, Energy Conversion 12 (1972) 65–68.
[9] Wei He, A simulation model for integrated molten carbonate fuel cell systems, Journal of Power Sources 49 (1994) 283–290.
[10] J.C. Amphlett, R.F. Mann, B.A. Peppley, P.R. Roberge, A. Rodrigues, A model predicting transient responses of proton exchange membrane fuel cells, Journal of Power Sources 61 (1996) 183–188.
[11] Helmut Lorenz, Karl-Ernst Noreikat, Thomas Klaiber, Wolfram Fleck, Josef Sonntag, Gerald Hornburg, Andreas Gaulhofer, Method and device for vehicle fuel cell dynamic power control, US Patent 5 646 852, July 1997, Assigned to Daimler-Benz Aktiengesellschaft.
[12] W. Edward Mufford, Douglas G. Strasky, Power control system for a fuel cell powered vehicle, US Patent 5 771 476, June 1998, Assigned to DBB Fuel Cell Engines GmbH.
[13] Rune L. Johansen, Fuel cells in vehicles. Master's thesis, Norwegian University of Science and Technology, 2003.
[14] Jay Tawee Pukrushpan, Modeling and control of fuel cell systems and fuel processors. PhD thesis, Department of Mechanical Engineering, University of Michigan, Ann Arbor, Michigan, USA, 2003.
[15] Jay Tawee Pukrushpan, Anna G. Stefanopoulou, Huei Peng, Modeling and control for PEM fuel cell stack system, in: American Control Conference, 2002, TP09-2.
[16] Maria Serra, Joaquín Aguado, Xavier Ansede, Jordi Riera, Controllability analysis of decentralised linear controllers for polymeric fuel cells, Journal of Power Sources 151 (2005) 93–102.
[17] S. Caux, J. Lachaize, M. Fadel, P. Shott, L. Nicod, Modelling and control of a fuel cell system and storage elements in transport applications, Journal of Process Control 15 (2005) 481–491.
[18] Phatiphat Thounthong, Stéphane Raël, Bernard Davat, Control strategy for fuel cell/supercapacitors hybrid power sources for electric vehicle, Journal of Power Sources 158 (2005) 806–814.
[19] Phatiphat Thounthong, Stéphane Raël, Bernard Davat, Test of a PEM fuel cell with low voltage static converter, Journal of Power Sources 153 (2006) 145–150.
[20] Song-Yul Choe, Jung-Gi Lee, Jong-Woo Ahn, Soo-Hyun Baek, Integrated modeling and control of a PEM fuel cell power system with a PWM DC/DC converter, Journal of Power Sources 164 (2007) 614–623.
[21] Federico Zenith, Control of Fuel Cells. PhD thesis, Norwegian University of Science and Technology, Trondheim, June 2007, URL http://urn.ub.uu.se/resolve?urn=urn:nbn:no:ntnu:diva-1537.
[22] G. Karimi, J.J. Baschuk, X. Li, Performance analysis and optimization of PEM fuel cell stacks using ow network approach, Journal of Power Sources 147 (2005) 162–177.
[23] Yuyao Shan, Song-Yul Choe, A high dynamic PEM fuel cell model with temperature effects, Journal of Power Sources 145 (2005) 30–39.
[24] Yuyao Shan, Song-Yul Choe, Modeling and simulation of a PEM fuel cell stack considering temperature effects, Journal of Power Sources 158 (2006) 274–286.

[25] European Economic Community, Council directive 91/441/EEC of 26 June 1991 amending directive 70/220/EEC on the approximation of the laws of the Member States relating to measures to be taken against air pollution by emissions from motor vehicles, June 1991, URL http://eur-lex.europa.eu/LexUriServ/LexUriServ.do?uri=CELEX:31991L0441:%EN:HTML.
[26] European Community, Commission directive 93/116/EC of 17 December 1993 adapting to technical progress council directive 80/1268/EEC relating to the fuel consumption of motor vehicles, December 1993, URL http://eur-lex.europa.eu/LexUriServ/LexUriServ.do?uri=CELEX:31993L0116:%EN:HTML.
[27] Jung-Tang Huang, Shao-Chang Cheng, Study of injection molding pressure sensor with low cost and small probe, Sensors and Actuators A: Physical 101 (2002) 269–274.
[28] Sigurd Skogestad, Simple analytic rules for model reduction and PID controller tuning, Journal of Process Control 13 (2003) 291–309.
[29] Kathy Sahner, Ralf Moos, Noriya Izu, Woosuck Shin, Norimitsu Murayama, Response kinetics of temperature-independent resistive oxygen sensor formulations: a comparative study, Sensors and Actuators B: Chemical 113 (2006) 112–119.
[30] Kousuke Yamamoto, Toshihiro Kasuga, Masayuki Nogami, An oxygen sensor based on copper(I)-conducting $CuTi_2$ $(PO_4)_3$ glass ceramics, Applied Physics Letters 73 (22) (1998) 3297–3299.
[31] F.R. Goldschmied, D.N. Wormley, Frequency response of blower/duct/plenum uid systems, Journal of Hydronautics 11 (1) (1977) 18–27.
[32] Franc Cimerman, Bogdan Blagojević, Ivan Bajsić, Identification of the dynamic properties of temperature-sensors in natural and petroleum gas, Sensors and Actuators A: Physical 96 (2002) 1–13.